



Article

# Snapin Specifically Up-Regulates $\text{Ca}_v1.3$ $\text{Ca}^{2+}$ Channel Variant with a Long Carboxyl Terminus

Sua Jeong <sup>1</sup>, Jeong-Seop Rhee <sup>2</sup>  and Jung-Ha Lee <sup>1,\*</sup>

<sup>1</sup> Department of Life Science, Sogang University, 35 Baekbeom-ro, Mapo-gu, Seoul 04107, Korea; sua jeong@sogang.ac.kr

<sup>2</sup> Synaptic Physiology Group, Department of Molecular Neurobiology, Max Planck Institute for Experimental Medicine, Hermann-Rein-Str. 3, 37075 Göttingen, Germany; rhee@em.mpg.de

\* Correspondence: jhleem@sogang.ac.kr; Tel.: +82-2-705-8791; Fax: +82-3-704-3601

**Abstract:**  $\text{Ca}^{2+}$  entry through  $\text{Ca}_v1.3$   $\text{Ca}^{2+}$  channels plays essential roles in diverse physiological events. We employed yeast-two-hybrid (Y2H) assays to mine novel proteins interacting with  $\text{Ca}_v1.3$  and found Snapin2, a synaptic protein, as a partner interacting with the long carboxyl terminus ( $\text{CT}_L$ ) of rat  $\text{Ca}_v1.3_L$  variant. Co-expression of Snapin with  $\text{Ca}_v1.3_L/\text{Ca}_v\beta_3/\alpha_2\delta_2$  subunits increased the peak current density or amplitude by about 2-fold in HEK-293 cells and *Xenopus* oocytes, without affecting voltage-dependent gating properties and calcium-dependent inactivation. However, the Snapin up-regulation effect was not found for rat  $\text{Ca}_v1.3_S$  containing a short CT ( $\text{CT}_S$ ) in which a Snapin interaction site in the  $\text{CT}_L$  was deficient. Luminometry and electrophysiology studies uncovered that Snapin co-expression did not alter the membrane expression of HA tagged  $\text{Ca}_v1.3_L$  but increased the slope of tail current amplitudes plotted against ON-gating currents, indicating that Snapin increases the opening probability of  $\text{Ca}_v1.3_L$ . Taken together, our results strongly suggest that Snapin directly interacts with the  $\text{CT}_L$  of  $\text{Ca}_v1.3_L$ , leading to up-regulation of  $\text{Ca}_v1.3_L$  channel activity via facilitating channel opening probability.

**Keywords:** snapin;  $\text{Ca}_v1.3$  L-type  $\text{Ca}^{2+}$  channel; two-electrode voltage clamping; whole-cell patch clamping; immunostaining; ON-gating current



**Citation:** Jeong, S.; Rhee, J.-S.; Lee, J.-H. Snapin Specifically Up-Regulates  $\text{Ca}_v1.3$   $\text{Ca}^{2+}$  Channel Variant with a Long Carboxyl Terminus. *Int. J. Mol. Sci.* **2021**, *22*, 11268. <https://doi.org/10.3390/ijms222011268>

Academic Editor: Masatoshi Maki

Received: 16 September 2021

Accepted: 15 October 2021

Published: 19 October 2021

**Publisher's Note:** MDPI stays neutral with regard to jurisdictional claims in published maps and institutional affiliations.



**Copyright:** © 2021 by the authors. Licensee MDPI, Basel, Switzerland. This article is an open access article distributed under the terms and conditions of the Creative Commons Attribution (CC BY) license (<https://creativecommons.org/licenses/by/4.0/>).

## 1. Introduction

External  $\text{Ca}^{2+}$  entry through voltage-activated  $\text{Ca}^{2+}$  channels (VACCs) acts as  $\text{Ca}^{2+}$  signals to mediate numerous physiological functions. VACCs are composed of a pore-forming  $\alpha_1$  subunit for  $\text{Ca}^{2+}$  entry and auxiliary subunits. Molecular cloning uncovered 10  $\text{Ca}^{2+}$  channel  $\alpha_1$  subunits, which determine primary electrophysiological and pharmacological characteristics of VACCs. In accordance with their electrophysiological and pharmacological properties as well as sequence similarity,  $\text{Ca}_v1.1$ – $\text{Ca}_v1.4$  are classified as L-type  $\text{Ca}^{2+}$  channels,  $\text{Ca}_v2.1$ – $\text{Ca}_v2.3$  as non-L-type  $\text{Ca}^{2+}$  channels, and  $\text{Ca}_v3.1$ – $\text{Ca}_v3.3$  as T-type  $\text{Ca}^{2+}$  channels [1].

The L-type channels play distinctive roles with different tissue distribution.  $\text{Ca}_v1.1$  acts as a voltage sensor in excitation-contraction coupling in skeletal muscle.  $\text{Ca}^{2+}$  influx through  $\text{Ca}_v1.2$  triggers contraction of cardiac and smooth muscle. Although  $\text{Ca}_v1.2$  and  $\text{Ca}_v1.3$  are commonly expressed in various tissues, their differential roles have been reported. For instance,  $\text{Ca}_v1.2$  mediates cardiac myocyte contraction in the heart, whereas  $\text{Ca}_v1.3$  contributes to pacemaker activity in the sinoatrial (SA) node [2,3]. In addition,  $\text{Ca}_v1.4$  is expressed predominately in the retina and was originally identified by its mutation being associated with congenital night blindness [4].

Studies of  $\text{Ca}_v1.3$  knock-out mice showed malfunction and degeneration of afferent auditory nerve fibers and hair cells, cardiac bradycardia arising from decreased pacemaker activity, hippocampal learning and memory impairment via reduced survival of new-born neurons, and insulin secretion reduction from pancreatic  $\beta$  cells [2,3,5,6]. More recently,

missense mutations in  $Ca_v1.3$  have been implicated in primary aldosteronism [7] and neuronal diseases, such as autism spectrum disorders and seizures [8,9]. Because of relatively low activation threshold, certain  $Ca_v1.3$  variants have been suggested as being low voltage-activated L-type  $Ca^{2+}$  channels and crucially involved in hormone secretion and certain neuronal excitability in response to low potential [10–13]. Indeed, the low-voltage activation of  $Ca_v1.3$  channels in post-synaptic neurons and adrenal chromaffin cells was found to trigger consecutive spikes and post-burst after-hyperpolarization via functional association with  $Ca^{2+}$ -activated  $K^+$  channels [12,14,15]. Furthermore,  $Ca_v1.3$  channels were reported to influence dendritic spine morphology and synaptic plasticity [8,16].

Snapin was initially found to associate with SNAP-25, a component of trans-SNARE complex in neuronal tissues to promote and stabilize SNARE complex assembly, leading to facilitation of synaptic transmission processes [17,18]. In spite of a challenging report in which the low expression and minor role of Snapin in neurons was addressed [19], Snapin deletion studies were shown to impair hormone secretion, synaptic vesicle fusion, and the homeostatic modulation of presynaptic vesicle release [20–22], supporting the facilitating effect of Snapin on synaptic transmission and hormone secretion. In non-neuronal cells, Snapin was found to be ubiquitously expressed and detected to interact with SNAP-23 [23]. As a component of BLOC1 (biogenesis of lysosome-related organelles) complex, Snapin was reported to contribute to the biogenesis of lysosome-related organelles and the intracellular transport of endocytosed materials for degradation [24,25]. Snapin, which mediates endo-lysosomal transport, was also involved in the recycling of synaptic vesicles in neuronal tissues [26]. Furthermore, the potential roles of Snapin have been greatly expanded with findings of its diverse interaction partners, including ryanodine receptor [27], water channels [28], TRPV1 [29], and  $Ca_v1.3$   $Ca^{2+}$  channel  $\alpha_1$  subunit [30]. In the latter report, Snapin1 co-expression in HEK-293 cells stably expressing  $Ca_v1.3$   $\alpha_1$  plus auxiliary subunits was shown to strongly reduce the peak current amplitude of  $Ca_v1.3$  channels. Similarly, Snapin1 overexpression in HL-1 cells was shown to profoundly reduce endogenous  $Ca_v1.3$  channel activity and protein. The Snapin-mediated ubiquitination of  $Ca_v1.3$  was addressed to be involved in the underlying mechanism for the reduction of  $Ca_v1.3$ .

Using yeast-two-hybrid (Y2H) screenings, in the present study, we attempted to mine molecular partners interacting with the long carboxyl terminus ( $CT_L$ ) of rat  $Ca_v1.3_L$  and isolate Snapin2, the broad roles of which were reviewed in the above paragraph. In contrast with a previous report [30], our reconstitution experiments of  $Ca_v1.3_L$  and Snapin in HEK-293 cells and *Xenopus* oocytes showed that Snapin co-expression similarly increased the channel activity of  $Ca_v1.3_L$  in the two systems, without changing voltage-dependent gating properties. Combined studies using immunocytochemistry and electrophysiology uncovered that the Snapin up-regulation of  $Ca_v1.3_L$  current arises from increased opening probability without changing surface expression.

## 2. Results

### 2.1. Snapin2 Is an Interaction Partner of Rat $Ca_v1.3_L$

We searched for novel molecular partners interacting with  $Ca_v1.3$   $Ca^{2+}$  channel, employing Y2H screening, for which the long carboxyl terminus (designated as  $CT_L$ , Figure 1A) of rat  $Ca_v1.3_L$  was used as bait, and a rat brain cDNA library was used as prey. A positive blue clone grown in a high-stringent condition ( $Ade^-$ ,  $Leu^-$ ,  $His^-$ ,  $Trp^-$ ) was isolated. The vector insert was sequenced and analyzed by BLAST, which identified that the DNA sequence contained the whole open-reading frame (82 amino acids) of rat Snapin2 (Genbank no. NM\_001025648). Sequence comparison (Figure 1D) showed that rat Snapin2 is a shorter variant than rat Snapin1 (136 amino acids). Notably, rat Snapin2 amino acid sequence approximately corresponds to the post half sequence (amino acid number 63 to 136) of rat Snapin1. When the  $CT_L$  and Snapin2 were co-transformed, positive blue colonies were formed in a high-stringent condition in the presence of X-gal, confirming their interaction (Figure 1B). Additional Y2H assays were conducted to examine whether

Snapin2 can interact with the other cytoplasmic structures of  $Ca_v1.3_L$ , including the amino-terminus (NT) and cytoplasmic loops connecting domains I, II, III, and IV (Figure 1A). It was determined that Snapin2 interacted with only the  $CT_L$  of  $Ca_v1.3_L$  but did not with the other cytoplasmic tail and loops (Figure 1C).

## 2.2. Up-Regulation of $Ca_v1.3_L$ Channel Activity by Snapin2 in HEK-293 Cells

To characterize the effects of Snapin2 on  $Ca_v1.3_L$ , Snapin2 was co-expressed with  $Ca_v1.3_L/Ca_v\beta_3/\alpha_2\delta_2$  by transfecting the cDNA constructs into HEK-293 cells. We recorded  $Ca_v1.3_L$  channel currents from HEK-293 cells using whole-cell patch clamping configuration from 48 h after transfection. Upon a series of 400-ms depolarizing step pulses ranging from  $-60$  mV to  $+70$  mV from a holding potential of  $-80$  mV, robust  $Ca^{2+}$  current traces were evoked from cells expressing  $Ca_v1.3_L/Ca_v\beta_3/\alpha_2\delta_2$  (Figure 2). The evoked  $Ca_v1.3_L$  currents were immediately activated upon serial step pulses, followed by rapidly decaying kinetics during the given period of test potentials, representing typical calcium-dependent inactivation (CDI) properties (Figure 2A). The current-voltage relationships (Figure 2B) obtained by plotting average current density values versus test potentials showed that the threshold potential was about  $-40$  mV, the potential inducing maximal peak current was  $0$  mV, and the reversal potential was around  $+70$  mV. These biophysical properties are quite similar to those reported previously [31]. Notably, the  $Ca^{2+}$  current densities over most of the test potentials were greatly facilitated by co-expression of Snapin2 with  $Ca_v1.3_L$  and auxiliary subunits (Figure 2A,B). The maximal peak current density values at  $0$  mV test potential were  $-62.3 \pm 11.9$  pA/pF for  $Ca_v1.3_L/Ca_v\beta_3/\alpha_2\delta_2$  (control) and  $-124.8 \pm 15.9$  pA/pF for co-expression of Snapin2, indicating that the Snapin2 approximately doubled the  $Ca_v1.3_L$  channel activity (Figure 2C). Similarly, the maximal chord conductance of  $Ca_v1.3_L$  channels was two-fold increased by Snapin2 ( $0.92 \pm 0.16$  vs.  $1.86 \pm 0.20$  nS/pF, Figure 2D). Besides the up-regulation in current density, we found that Snapin2 co-expression induced no significant alterations in other biophysical properties, including voltage-dependent gating properties and CDI (Figure 2E–G; Table 1).

**Table 1.** Summary of biophysical properties of  $Ca_v1.3$  channels co-expressed with Snapin.

	$V_{50,act}$ (mV)	Slope (k)	$V_{50,inact}$ (mV)	Slope (k)	n	Maximal Current Density (pA/pF)	System
$Ca_v1.3_L/\beta_3/\alpha_2\delta_2$	$-16.0 \pm 0.3$	$7.3 \pm 0.3$	$-39.2 \pm 0.3$	$-4.1 \pm 0.3$	18~21	$-63.8 \pm 6.4$	HEK-293 cell
+Snapin 2	$-16.2 \pm 0.5$	$7.1 \pm 0.4$	$-38.9 \pm 0.5$	$-4.6 \pm 0.5$	12~15	$-124.8 \pm 15.9$ (**)	
+Snapin 1	$-15.9 \pm 0.3$	$7.0 \pm 0.3$	$-39.0 \pm 0.4$	$-4.0 \pm 0.4$	10	$-135.7 \pm 21.2$ (**)	
$Ca_v1.3_S/\beta_3/\alpha_2\delta_2$	$-14.2 \pm 0.3$	$6.9 \pm 0.2$	$-38.3 \pm 0.3$	$-3.9 \pm 0.3$	8	$-92.1 \pm 10.2$	
+Snapin 2	$-14.3 \pm 0.8$	$7.0 \pm 0.7$	$-38.4 \pm 0.4$	$-3.9 \pm 0.3$	8	$-89.3 \pm 11.9$	
$Ca_v1.3_L/\beta_3$	$-18.4 \pm 0.8$	$9.8 \pm 0.8$	$-47.8 \pm 1.5$	$-5.8 \pm 1.3$	17~20	$-1271.1 \pm 164.8$ nA	<i>Xenopus</i>
+Snapin 2	$-19.5 \pm 1.0$	$9.5 \pm 0.9$	$-47.2 \pm 1.8$	$-5.7 \pm 1.6$	17~20	$-2100.5 \pm 209.7$ nA (**)	oocyte

Data are presented as mean  $\pm$  S.E.M. Significance levels were evaluated using Student's *t*-test or one-way ANOVA combined with Turkey's multiple comparison test;  $p < 0.01$  (\*\*).

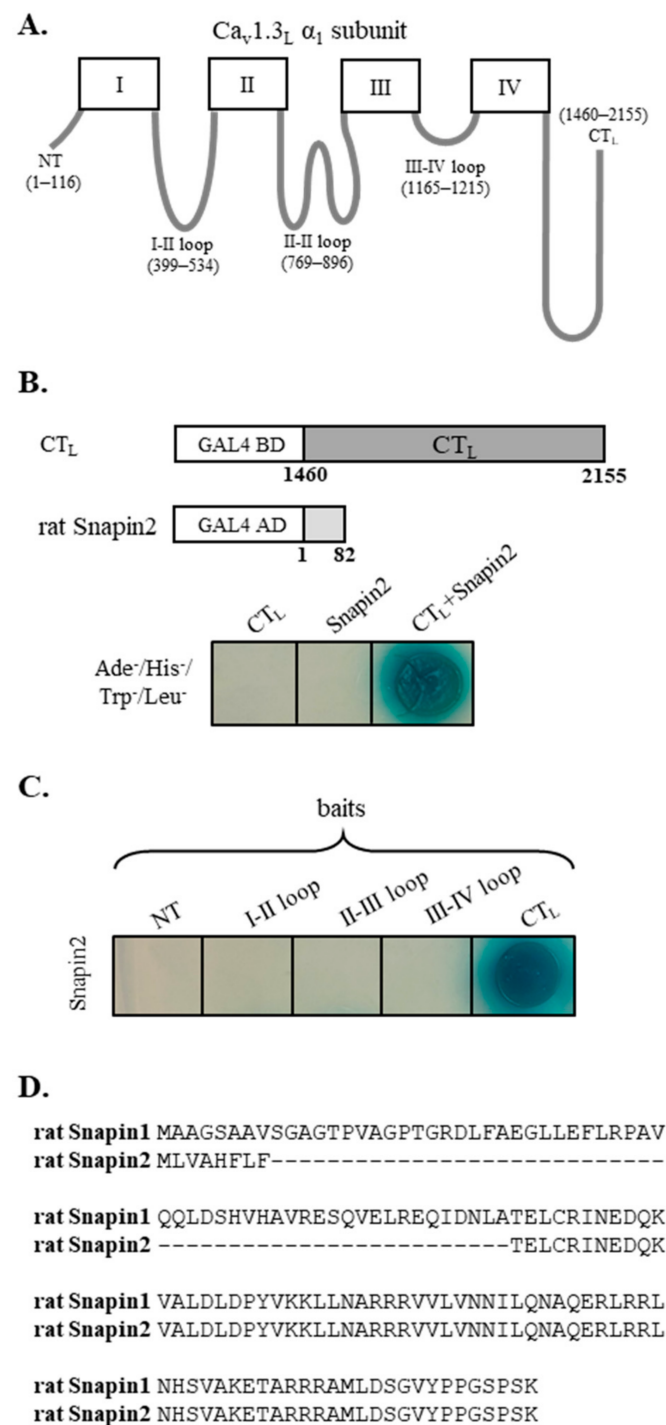


**Figure 1.** Isolation of rat Snapin2 as an interaction partner with the CT<sub>L</sub> of rat Ca<sub>v</sub>1.3 by yeast-two-hybrid (Y2H) screenings. **(A)** Schematic diagram of rat Ca<sub>v</sub>1.3<sub>L</sub> α<sub>1</sub> subunit. The amino acid numbers for the intracellular structures of rat Ca<sub>v</sub>1.3<sub>L</sub> α<sub>1</sub> subunit, including NT (amino terminus), I-II, II-III, III-IV, and CT<sub>L</sub> are designated in parentheses. **(B)** Y2H data representing an interaction between the CT<sub>L</sub> and rat Snapin2. A positive clone containing rat Snapin2 construct was isolated from Y2H screenings for which the CT<sub>L</sub> and a rat brain library were used as bait and prey, respectively. Co-transformation of the CT<sub>L</sub> and rat Snapin2 produced a blue colony in a high-stringent condition (−Ade, −His, −Leu, and −Trp) with X-gal. **(C)** Y2H results illustrating that rat Snapin2 interacted with only the CT<sub>L</sub> but not with the other intracellular structures. **(D)** Amino acid sequence alignment between rat Snapin1 and Snapin2.

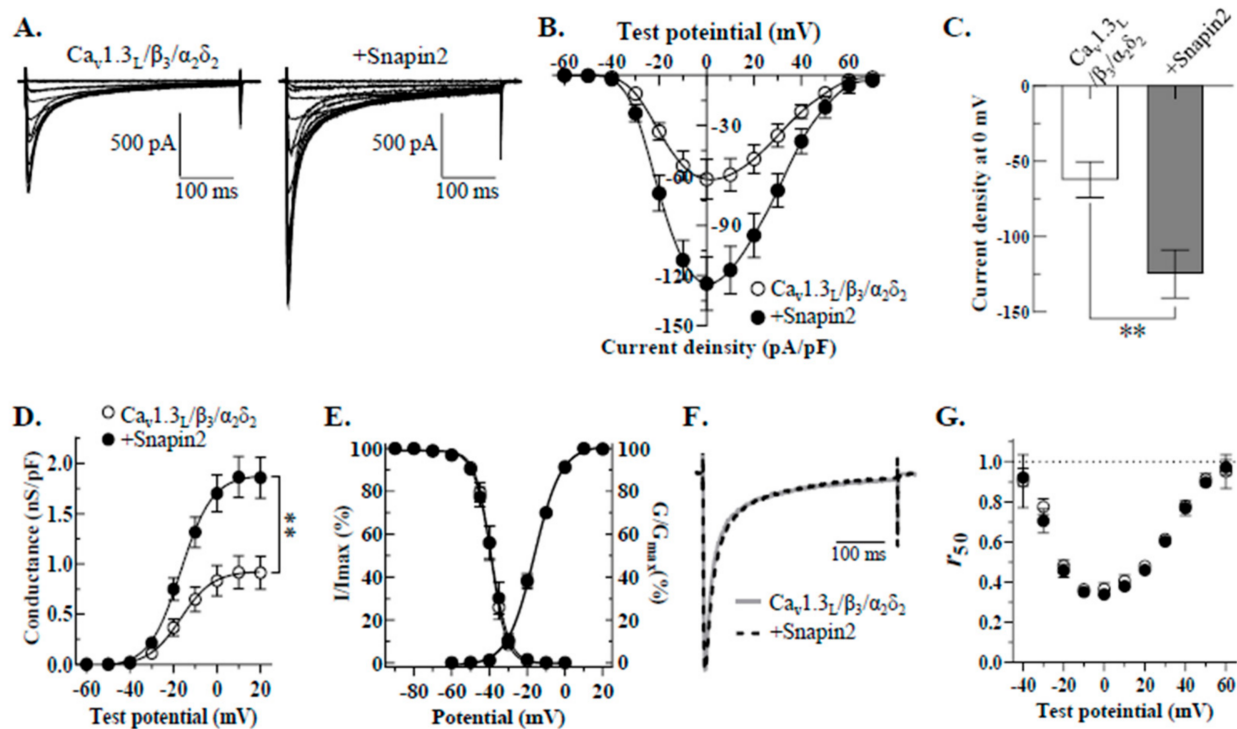


**Figure 2.** Up-regulation of  $\text{Ca}_v1.3_L$  channel activity by Snapin2 in HEK-293 cells. (A) Representative  $\text{Ca}^{2+}$  current traces through  $\text{Ca}_v1.3_L$  channels co-expressed without (left) or with Snapin2 (right).  $\text{Ca}_v1.3_L$ ,  $\beta_3$ , and  $\alpha_2\delta_2$  cDNA constructs were transfected into HEK-293 cells (left) and co-transfected with rat Snapin2 cDNA construct in an equal molar ratio (right). In 10 mM  $\text{Ca}^{2+}$  solution,  $\text{Ca}^{2+}$  current traces through  $\text{Ca}_v1.3_L$  channels were evoked by application of an  $I$ - $V$  protocol consisting of 400-ms depolarizing step pulses from  $-60$  mV to  $+70$  mV by 10 mV increments from a holding potential of  $-80$  mV. (B,C)  $I$ - $V$  relationships of  $\text{Ca}_v1.3_L$  channels co-expressed without or with Snapin2. Current density values (pA/pF) obtained by dividing the peak current amplitude values of  $\text{Ca}_v1.3$   $\text{Ca}^{2+}$  currents evoked at various test potentials by cell capacitance were averaged and then plotted against test potentials ( $n = 13$ – $15$ ). (C) The maximal peak current density values of  $\text{Ca}_v1.3_L$  channels co-expressed without or with Snapin2 measured at 0 mV test potential are represented as bar graphs ( $-62.3 \pm 11.9$  vs.  $-124.8 \pm 15.9$  pA/pF;  $n = 13$ – $15$ ; Student's unpaired  $t$ -test,  $p < 0.01$ , \*\*). (D) Snapin2 effect on the chord conductance of  $\text{Ca}_v1.3_L$  channels. The chord conductance values of  $\text{Ca}_v1.3_L$  channels without or with Snapin2 were normalized to the cell capacitance, and average values were plotted against test potentials. Snapin2 co-expression increased the maximal conductance of  $\text{Ca}_v1.3_L$  by roughly 1.9-fold at 10 mV ( $0.9 \pm 0.2$  vs.  $1.9 \pm 0.2$  nS/pF;  $n = 13$ – $15$ ; Student's unpaired  $t$ -test,  $p < 0.01$ , \*\*). (E) Snapin2 effect on voltage-dependent channel activation and channel availability of  $\text{Ca}_v1.3_L$  channels. The chord conductance values of  $\text{Ca}_v1.3_L$  channels without or with Snapin2 were normalized and superimposed ( $n = 13$ – $15$ ). Channel availability of  $\text{Ca}_v1.3_L$  channels was evaluated by a two-step pulse protocol consisting of 10-s pre-conditioning pulses ranging from  $-90$  mV to 0 mV by an increment of 10 mV, followed by a step pulse to 0 mV. Currents measured at 0 mV test potential were normalized to the current amplitude after a preconditioning potential of  $-90$  mV and plotted against pre-pulse potentials. The average percentage data were fit to the Boltzmann equation ( $n = 10$ – $12$ ). (F,G) Snapin2 effect on CDI of  $\text{Ca}_v1.3_L$  channels. (F)  $\text{Ca}_v1.3_L$   $\text{Ca}^{2+}$  current traces through  $\text{Ca}_v1.3_L$  channels without or with Snapin2 at 0 mV test potential were normalized and superimposed, exhibiting little difference in CDI. (G) Snapin effect on  $r_{50}$ . The  $r_{50}$  values (the fractions of  $\text{Ca}^{2+}$  peak currents remaining after 50 ms;  $n = 7$ – $8$ ) of  $\text{Ca}_v1.3_L$  channels without or with Snapin2 were plotted against test potentials. The  $r_{50}$  values were not altered by Snapin2. No differences in the  $r_{350}$  values were detected (data not shown).

### 2.3. The Snapin2 Up-Regulation Effect on $\text{Ca}_v1.3_L$ Channel Was Reproduced in *Xenopus* Oocytes

We also examined whether Snapin2 can modulate  $\text{Ca}_v1.3_L$  channel activity in *Xenopus* oocytes, an expression system quite different from HEK-293 cells.  $\text{Ca}_v1.3_L/\text{Ca}_v\beta_3$  were co-expressed with or without Snapin2 by injection of their cRNAs in equal molar ratio. On the 4th day after cRNA injection, expression of  $\text{Ca}_v1.3_L$  channels in oocytes was detected as robust  $\text{Ba}^{2+}$  currents in response to the  $I$ - $V$  voltage protocol (Figure 3A). The  $I$ - $V$

relationships obtained by plotting average peak current amplitudes against test potentials showed that average peak current amplitudes recorded from oocytes co-expressing Snapin2 with  $\text{Ca}_v1.3_L/\beta_3$  were about 2-fold greater at  $-10$  mV test potential than those from the control oocytes expressed with  $\text{Ca}_v3.1_L/\beta_3$  ( $-2414.5 \pm 314.6$  vs.  $-1271.1 \pm 214.1$  nA) (Figure 3B,C). Comparison of chord conductance displayed that Snapin2 similarly increased the maximal chord conductance of  $\text{Ca}_v1.3_L$  channels ( $14.6 \pm 2.6$  vs.  $28.1 \pm 2.9$   $\mu\text{S}$ ) (Figure 2D). Similar increments were detected at other test potentials, but no significant alterations in voltage-dependent gating properties were induced by co-expression of Snapin2 (Figure 3E and Table 1). Taken together, our findings that Snapin2 similarly up-regulated  $\text{Ca}_v1.3_L$  channel activity in two different expression systems implies that, regardless of cell type, the interaction of Snapin2 with the  $\text{CT}_L$  of  $\text{Ca}_v1.3_L$  can increase  $\text{Ca}_v1.3_L$  channel activity. Consequently, the up-regulation of calcium influx through  $\text{Ca}_v1.3_L$  channels by Snapin2 might affect related physiological events.

#### 2.4. Lack of the Snapin2 Up-Regulation Effect on $\text{Ca}_v1.3_S$ Variant

We next investigated whether Snapin2 can regulate  $\text{Ca}_v1.3_S$  variant containing a short CT. Co-expression of Snapin2 with  $\text{Ca}_v1.3_S/\beta_3/\alpha_2\delta_2$  did not show any alterations in the peak current density of  $\text{Ca}_v1.3_S$  channels and other biophysical properties, including  $I$ - $V$  relationship, CDI, and gating properties (Figure 4; Table 1). The differential regulatory effects by Snapin2 are likely to depend on the structural difference of CT tails. In order to find out in detail any differential regulation resulting from differences in the CT tails, we tested whether Snapin2 can interact with the short CT (designated as “ $\text{CT}_S$ ”) of  $\text{Ca}_v1.3_S$  using Y2H assays. It was determined that the  $\text{CT}_S$  did not interact with Snapin2 (Figure 5A).

Subsequently we dissected the  $\text{CT}_L$  into multiple fragments and cloned them into bait vector to localize the Snapin2 interacting site in the  $\text{CT}_L$  using Y2H assays (Figure 5B). Systematic Y2H assays narrowed down a Snapin2 interaction site to be C6-2 comprised of 24 amino acids (YYNRYPGSSMDFERPRGYHHPQGF) (Figure 5B). Analysis of the amino acid sequence revealed that it pertained to the translated sequence of exon 44 (Figure 5C). These results strongly suggest that Snapin2 specifically interacts with long C-terminal  $\text{Ca}_v1.3$  variants containing exon 44 and explains why  $\text{Ca}_v1.3_S$  variant deficient of exon 44 was not up-regulated by Snapin2.

#### 2.5. The Snapin2 Up-Regulation of $\text{Ca}_v1.3_L$ Channel Activity Was Reproduced by Snapin1

A previous study using Y2H and GST pull-down assays reported that Snapin1, a longer variant than Snapin2, interacted with the  $\text{CT}_L$  of human  $\text{Ca}_v1.3_L$  variant [30]. In contrast with our patch-clamping results showing that Snapin2 co-expression up-regulated  $\text{Ca}_v1.3_L$  channel activity, Sun and his colleagues showed that Snapin1 co-expression strongly down-regulated  $\text{Ca}_v1.3$  channel activity in HEK-293 cells and HL-1 cells.

Because these contradictory results might arise from different regulation by the two Snapin variants co-expressed, we cloned rat Snapin1 cDNA (by RT-PCR from rat brain total RNA; refer to the method section) to examine the regulatory effects of Snapin1 on  $\text{Ca}_v1.3_L$  channels. In HEK-293 cells Snapin1 and  $\text{Ca}_v1.3_L/\beta_3/\alpha_2\delta_2$  were co-expressed by transfection of their constructs. In response to the  $I$ - $V$  protocol,  $\text{Ca}_v1.3_L$  channel currents were evoked from HEK cells under similar experimental conditions and showed that the  $\text{Ca}_v1.3_L$   $\text{Ca}^{2+}$  current density ( $-69.2 \pm 11.0$  vs.  $-135.7 \pm 17.6$  pA/pF) and maximal chord conductance ( $1.0 \pm 0.2$  vs.  $2.1 \pm 0.3$  nS/pF) were approximately 2-fold up-regulated by Snapin1 (Figure 6B–D). In contrast, the CDI and voltage-dependent gating properties were little changed (Figure 6E–G). The results show that the up-regulation of  $\text{Ca}_v1.3_L$  channel activity by Snapin1 is quite similar to that by Snapin2. We also tested whether  $\text{Ca}_v1.3_S$  channel can be affected by co-expression of Snapin1. It turned out that Snapin1 did not alter the current density and other biophysical properties of  $\text{Ca}_v1.3_S$  channel (Supplementary Figure S1). This implies that Snapin1 is likely not to interact with  $\text{Ca}_v1.3_S$ . These findings strongly suggest that both of the Snapin isoforms can facilitate the  $\text{Ca}_v1.3_L$  channel activity in a similar manner via an association with the CT of  $\text{Ca}_v1.3_L$ .

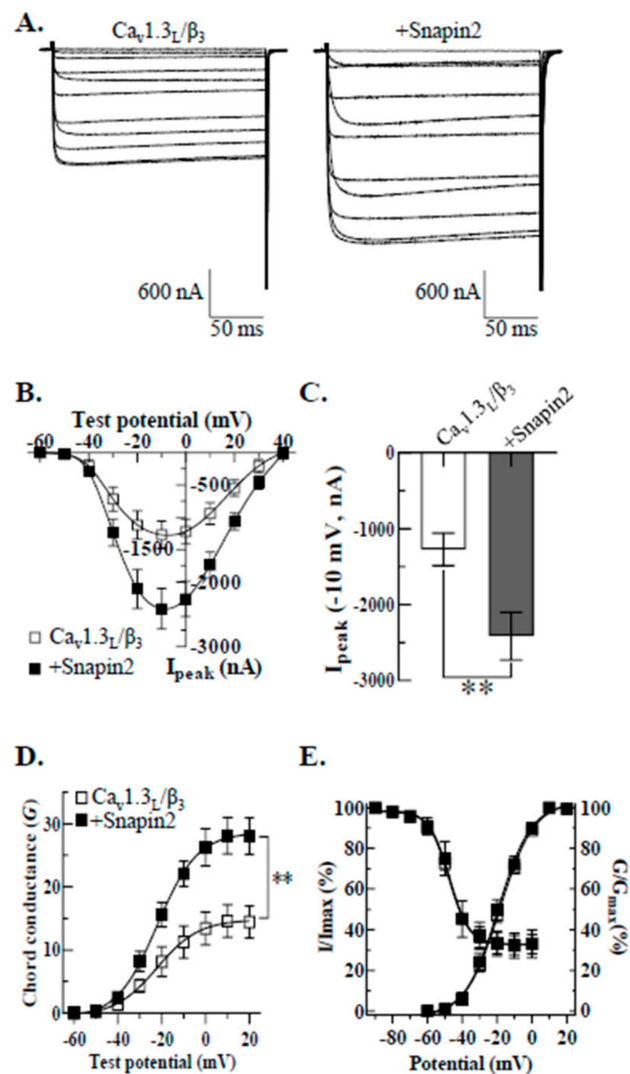


**Figure 3.** Snapin2 co-expression up-regulated  $Ca_v1.3_L$  channel activity in *Xenopus* oocytes. (A) Representative current traces of  $Ca_v1.3_L$  and  $Ca_v\beta_3$  co-expressed without (left) or with Snapin2 (right) recorded in 10 mM  $Ba^{2+}$  solution. Current traces were evoked by an  $I$ - $V$  protocol consisting of 200-ms depolarizing step pulses from  $-60$  mV to  $+40$  mV from a holding potential of  $-80$  mV. (B,C),  $I$ - $V$  relationships of  $Ca_v1.3_L$  channels without or with Snapin2. (B) Average peak current amplitude values of  $Ca_v1.3_L$  without ( $\square$ ) or with Snapin2 ( $\blacksquare$ ) were plotted against test potentials ( $n = 20$ – $23$ ). (C) The average peak current amplitude values of  $Ca_v1.3_L$  channels at  $-10$  mV test potential are represented as bar graphs ( $-1271.1 \pm 214.1$  vs.  $-2414.5 \pm 314.6$  nA;  $n = 20$ – $23$ ; Student's unpaired  $t$ -test,  $p < 0.01$ , \*\*). (D) Chord conductance of  $Ca_v1.3_L$  channels co-expressed without ( $\square$ ) or with Snapin2 ( $\blacksquare$ ). Snapin2 co-expression enhanced about 1.9-fold the maximum chord conductance values ( $14.6 \pm 2.6$  vs.  $28.1 \pm 2.9$  nS;  $n = 20$ ; Student's unpaired  $t$ -test,  $p < 0.01$ , \*\*). (E) Snapin2 effect on voltage-dependent channel activation and channel availability of  $Ca_v1.3_L$  channels. The chord conductance values of  $Ca_v1.3_L$  channels without ( $\square$ ) or with Snapin2 ( $\blacksquare$ ) were normalized to the maximal chord conductance and superimposed. A similar two-step pulse protocol was applied to evaluate channel availability of  $Ca_v1.3_L$  channels without ( $\square$ ) or with Snapin2 ( $\blacksquare$ ). Normalized data for channel availability were plotted against pre-pulse potentials, and the smooth curves were from fitting the data to the Boltzmann equation ( $n = 20$  for activation,  $n = 17$  for channel availability).

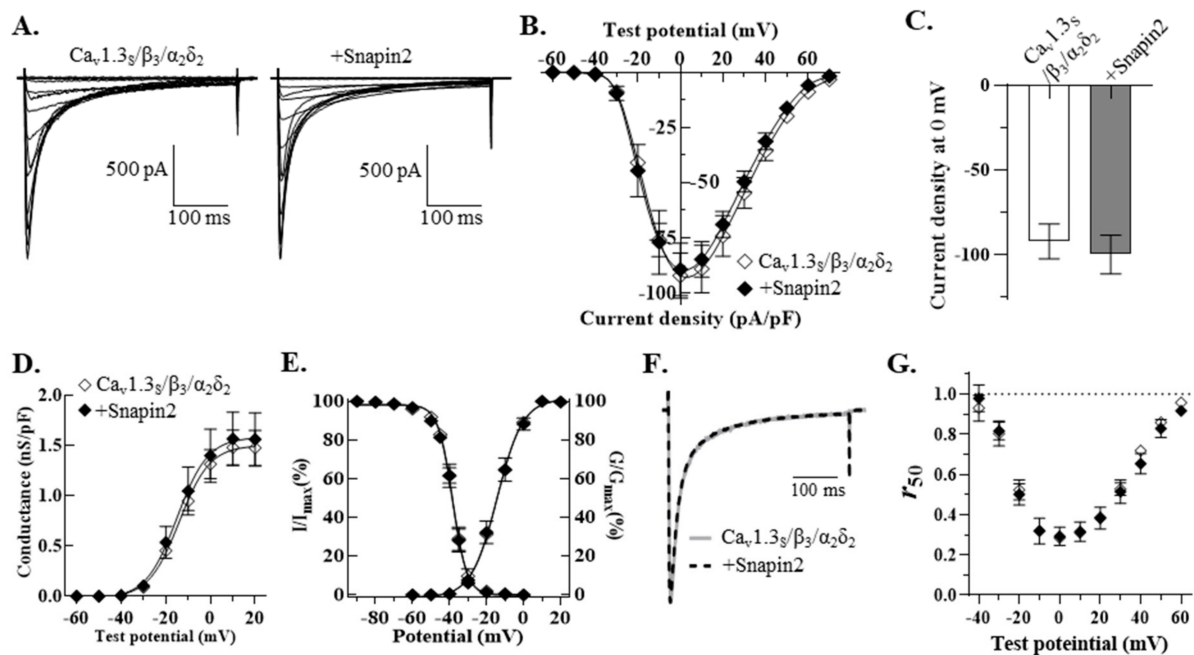


**Figure 4.** No regulatory effect of Snapin2 on  $Ca_v1.3_S$ . (A) Representative current traces through  $Ca_v1.3_S/\beta_3/\alpha_2\delta_2$  co-expressed without (left) or with Snapin2 (right).  $Ca_v1.3_S$  current traces were evoked in response to the  $I$ - $V$  protocol (described in Figure 2) in 10 mM  $Ca^{2+}$  solution. (B,C)  $I$ - $V$  relationships of  $Ca_v1.3_S$  channels without ( $\diamond$ ) or with Snapin2 ( $\blacklozenge$ ). Average current density values (pA/pF) were plotted against test potentials ( $n = 8$ ). (C) The average peak current density values at 0 mV test potential are represented as bar graphs ( $-92.1 \pm 10.2$  vs.  $-89.3 \pm 11.9$  pA/pF;  $n = 8$ ). (D) No effect of Snapin2 on the chord conductance of  $Ca_v1.3_S$  channels. The chord conductance values were normalized to the cell capacitance and plotted against test potentials ( $1.5 \pm 0.2$  vs.  $1.6 \pm 0.3$  nS/pF;  $n = 8$ ). (E) Activation and channel availability curves of  $Ca_v1.3_S$  channels co-expressed without or with Snapin2. Activation and channel availability curves of  $Ca_v1.3_S$  channels were obtained by the same methods in Figure 2 legend ( $n = 8$ ). (F) Snapin2 effect on the CDI of  $Ca_v1.3_S$  channels.  $Ca_v1.3_S$   $Ca^{2+}$  current traces elicited at 0 mV test potential were superimposed, exhibiting no difference in CDI. (G) No alteration in the  $r_{50}$  value of  $Ca_v1.3_S$ . The  $r_{50}$  values of  $Ca_v1.3_S$  channels ( $\pm$ Snapin2) were plotted against test potentials ( $n = 5$ ). No differences in the  $r_{350}$  values were detected (data not shown).

## 2.6. No Effect of Snapin on Membrane and Total Expression of $Ca_v1.3_L$ Channels

We engineered to fuse hemagglutinin (HA) epitope at the extracellular S5-pore loop of domain II of  $Ca_v1.3_L$  (Figure 7A; refer to the method section) to examine whether the membrane and total expression of  $Ca_v1.3_L$  channels can be changed by Snapin2. After  $Ca_v1.3_L$ -HA/ $\beta_3/\alpha_2\delta_2$  were co-expressed with or without Snapin2 in HEK-293 cells, membrane  $Ca_v1.3_L$ -HA channels and total  $Ca_v1.3_L$ -HA were quantitated by measuring luminescence intensity of multiple groups of non-permeabilized and permeabilized HEK-293 cells, respectively. Analysis of data showed that both the membrane expression and the total expression of  $Ca_v1.3_L$ -HA channels in HEK-293 cells were little changed by co-expression of Snapin2 (Figure 7B,C). Consistently, the normalized ratio of membrane  $Ca_v1.3_L$ -HA to total  $Ca_v1.3_L$ -HA was not affected by co-expression of Snapin2 (Figure 7D), supporting that Snapin2 does not affect the membrane and total expression of  $Ca_v1.3_L$  channels.

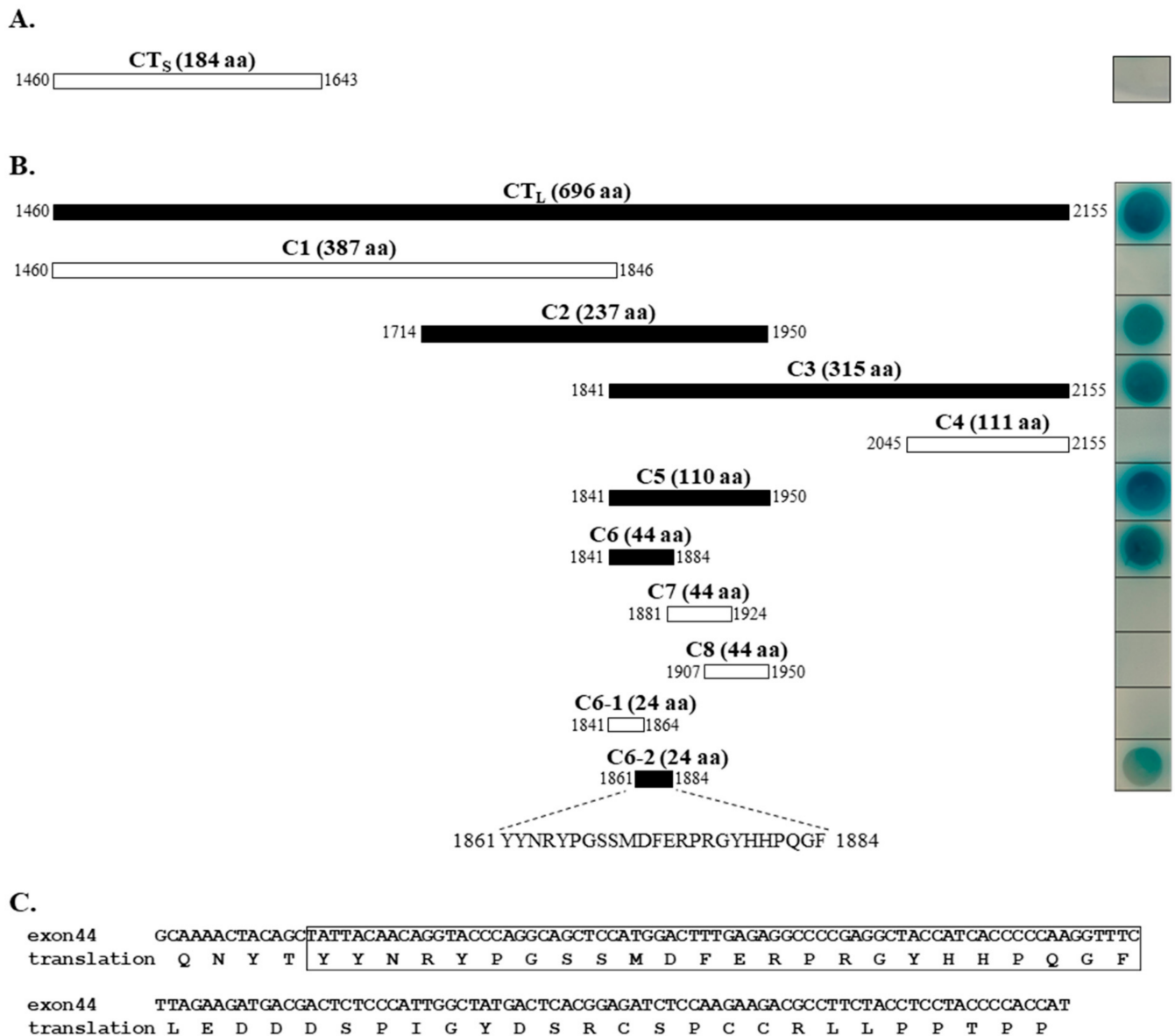


**Figure 5.** Identification of a Snapin2 interaction site in Ca<sub>v</sub>1.3 CT tails using Y2H assays. (A) No interaction of the CT<sub>S</sub> of rat Ca<sub>v</sub>1.3<sub>S</sub> with Snapin2, based on Y2H assays. The CTs of rat Ca<sub>v</sub>1.3<sub>S</sub> are shown schematically as a white box with amino acid numbers and size. No blue colony was formed by Y2H assay (right). (B) Localization of a Snapin2 association site in the CT<sub>L</sub> of Ca<sub>v</sub>1.3<sub>L</sub>. The CT<sub>L</sub> of Ca<sub>v</sub>1.3<sub>L</sub> is shown as a black box representing its association with Snapin2. The CT<sub>L</sub> (1460–2155) was divided into C1 to C4. The overlapped region between C2 and C3 was designated as C5 (1841–1950), which was subsequently dissected into C6 to C8. C6 was finally divided into C6-1 and C6-2. C6-2 (YYNRYPGSSMDFERPRGYHHPQGF) was localized to interact with Snapin2. Blue colonies grown in a stringent condition (lacking Ade, His, Leu, and Trp) treated with X-gal were exhibited in the right side of the diagram. (C) Sequence information of C6-2 and exon44. The amino acid sequence of C6-2 marked as a box belongs to the deduced sequence of exon44.

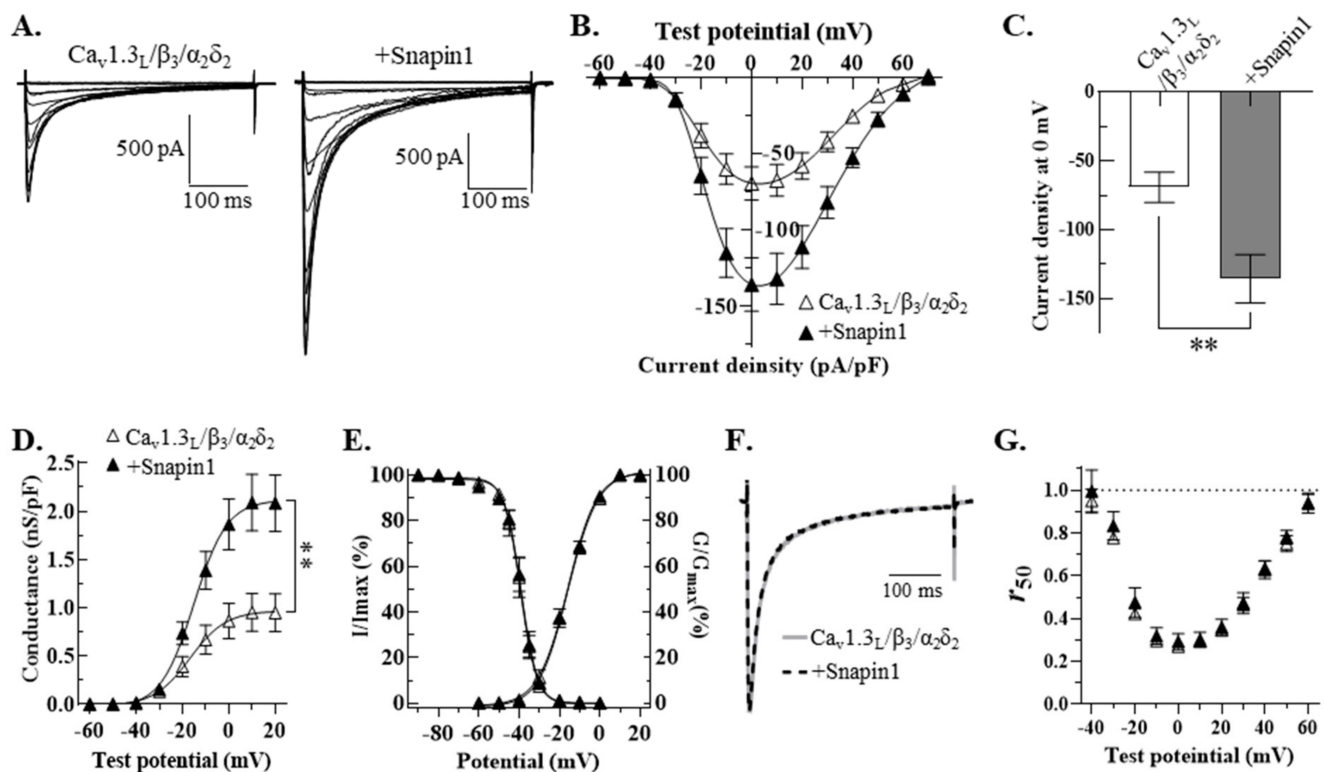


**Figure 6.** Up-regulation effect of Snapin1 variant on  $Ca_v1.3_L$  channels. (A)  $Ca_v1.3_L/\beta_3/\alpha_2\delta_2$  without (left) or with (right) Snapin1 were co-expressed in HEK-293 cells. The same voltage protocols and analysis described in Figure 2 were used to characterize the biophysical properties of  $Ca_v1.3_L$  channels. (B) The  $I$ - $V$  relationships of  $Ca_v1.3_L/\beta_3/\alpha_2\delta_2$  co-expressed with (▲) or without (△) Snapin1 ( $n = 8$ ). (C) Snapin1 effect on the maximal current density of  $Ca_v1.3_L$ . The maximal current density values of  $Ca_v1.3_L$  without or with Snapin1 are  $-69.2 \pm 11.0$  pA/pF and  $-135.7 \pm 17.6$  pA/pF ( $n = 10$ ; Student's unpaired  $t$ -test,  $p < 0.01$ , \*\*). (D) The chord conductance of  $Ca_v1.3_L$  channels without (△) or with (▲) Snapin1. The maximal normalized conductance values of  $Ca_v1.3_L$  without or with Snapin1 are  $0.95 \pm 0.20$  and  $2.09 \pm 0.29$  nS/pF ( $n = 10$ ; Student's unpaired  $t$ -test,  $p < 0.01$ , \*\*). (E) Channel availability and activation curves of  $Ca_v1.3_L$  channels without (△) or with (▲) Snapin1 ( $n = 10$ ). (F,G) No alteration in the CDI of  $Ca_v1.3_L$  by Snapin1.  $Ca^{2+}$  current traces through  $Ca_v1.3_L$  channels without or with Snapin1 evoked at 0 mV test potential were superimposed. The  $r_{50}$  values (G) of  $Ca_v1.3_L$  channels in the presence or absence of Snapin1 at various test potentials did not change the CDI of  $Ca_v1.3_L$  channels ( $n = 7$ ).

To directly observe immunofluorescence images for their surface expression, we also performed immunocytochemistry staining experiments with HA antibodies and FITC conjugated secondary antibodies. Confocal microscopy exhibited little detection of fluorescence images taken from the control cells transfected with empty vector (left panel of Figure 7E). In contrast, there was strong detection of fluorescence images from the cells expressing  $Ca_v1.3_L$ -HA /  $\beta_3/\alpha_2\delta_2$  with or without Snapin2 (middle and right panels of Figure 7E), thereby indicating great surface expression of  $Ca_v1.3_L$ -HA channels. Notably, the membrane expression of  $Ca_v1.3_L$ -HA channels with or without co-expression of Snapin2 appeared to be comparable. When the fluorescence intensity of membrane  $Ca_v1.3_L$  expression was quantitated using line-scanning analysis, the whole line-scan profiles for the membrane  $Ca_v1.3_L$  expression with or without co-expression of Snapin2 were almost overlapped (Figure 7F). Analysis of data showed that the maximal fluorescence intensity in the plasma membrane was also comparable with or without Snapin2 ( $70.3 \pm 5.3$  vs.  $73.7 \pm 6.6$  a.u.; Figure 7G). Taken together, these immunostaining results are in good agreement with the results from the luminometry experiments, strongly suggesting that co-expression of Snapin does not affect the surface expression and total expression of  $Ca_v1.3_L$  channels.

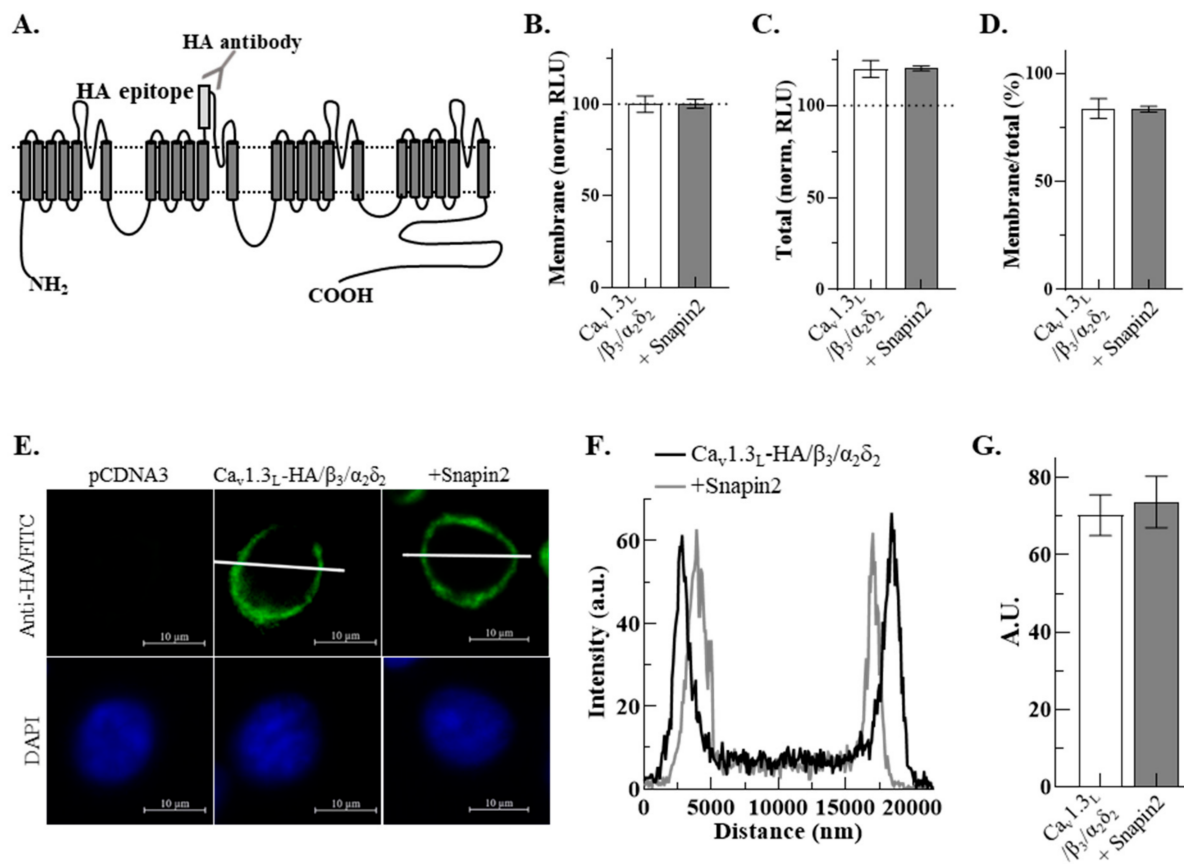


**Figure 7.** The surface and total expression of Ca<sub>v</sub>1.3<sub>L</sub> channels was not changed by Snapin2. (A) Schematic diagram of Ca<sub>v</sub>1.3<sub>L</sub>-HA. The HA epitope was tagged at the extracellular S5-pore loop of Ca<sub>v</sub>1.3<sub>L</sub> domain II (refer to the method section). (B–D) Luminometric quantification of expression levels of Ca<sub>v</sub>1.3<sub>L</sub>-HA without or with Snapin2. (B) Surface expression measured in non-permeabilized HEK-293 cells expressing Ca<sub>v</sub>1.3<sub>L</sub>-HA/β<sub>3</sub>/α<sub>2</sub>δ<sub>2</sub> without or with Snapin2. The luminescence intensities (arbitrary unit) were  $3.75 \times 10^7 \pm 0.25 \times 10^7$  and  $3.86 \times 10^7 \pm 0.20 \times 10^7$  (n = 8). Their normalized values (relative luminescence unit, RLU) are represented as bar graphs. (C) Total expression measured in permeabilized HEK-293 cells expressing Ca<sub>v</sub>1.3<sub>L</sub>-HA/β<sub>3</sub>/α<sub>2</sub>δ<sub>2</sub> without or with Snapin2. The luminescence values of total expression are  $3.95 \times 10^7 \pm 0.05 \times 10^7$  and  $4.35 \times 10^7 \pm 0.20 \times 10^7$  (n = 8). RLU values were obtained by normalizing luminescence values to the non-permeabilized Ca<sub>v</sub>1.3<sub>L</sub>-HA/β<sub>3</sub>/α<sub>2</sub>δ<sub>2</sub> signal. (D) Ratios of surface/total expression are represented as bar graphs. The ratios are not significantly different between with or without Snapin2. (E) Confocal microscopy images of surface expression of Ca<sub>v</sub>1.3<sub>L</sub>-HA without or with Snapin2. A set of HEK-293 cells transfected with Ca<sub>v</sub>1.3<sub>L</sub>-HA/β<sub>3</sub>/α<sub>2</sub>δ<sub>2</sub> without or with Snapin2 was stained with anti-HA antibodies and then FITC conjugated secondary antibodies. The middle and right panels show representative fluorescence images for Ca<sub>v</sub>1.3<sub>L</sub>-HA with or without Snapin2 (n = 3). The negative control image was from cells transfected with pCDNA3 vector (left panel). DAPI stained images of corresponding cells are shown in the lower panels. (F) Line-scanning analyses of Ca<sub>v</sub>1.3<sub>L</sub>-HA expression. Representative line-scan profiles of cells expressing Ca<sub>v</sub>1.3<sub>L</sub>-HA without (black line) or with Snapin2 (gray line) were obtained by a software program provided by ZEISS. (G) The maximal intensity values (arbitrary unit, a.u.) across the cells are represented as bar graphs, showing no statistically significant difference ( $70.3 \pm 5.3$  and  $73.7 \pm 6.6$  a.u.; n = 10).

### 2.7. Snapin Up-Regulation of Ca<sub>v</sub>1.3<sub>L</sub> Activity Comes from Enhanced Opening Probability

Whole-cell current (*I*) can be described by the multiplication of the number of channels (*n*), their opening probability (*P*<sub>o</sub>), and the channel's unitary conductance (*i*). Based on this relationship ( $I = nP_o i$ ), the increase of Ca<sub>v</sub>1.3<sub>L</sub> activity (*I*) induced by co-expression of Snapin2, could be generated by changes of one or more parameters. To explore the underlying mechanism for the Snapin2 up-regulation of Ca<sub>v</sub>1.3<sub>L</sub> activity, we attempted to measure ON-gating currents at the virtual reversal potential for the Ca<sup>2+</sup> currents and ionic tail currents from the same cells where ON-gating currents (*Q*<sub>ON</sub>) are proportional

to the number of channels in the plasma membrane and ionic tail currents ( $I_{tail}$ ) upon repolarization represent the whole channel activity ( $I$ ) [32]. In general, we observed that Snapin co-expression produced larger tail currents against comparable ON-gating currents (Figure 8A). The  $Q_{ON}$  values obtained from integrating the areas under the ON-gating currents were plotted against tail current amplitude values from the same cells. Regression analysis of data yielded slopes, which represent approximate estimates of opening probability ( $P_o$ ) (Figure 8B). It turned out that the slopes were about 2-fold increased by co-expression of Snapin1 or Snapin2, indicating that the  $P_o$  of  $Ca_v1.3_L$  channels was significantly enhanced by Snapin1 or 2 ( $p < 0.0001$ , \*\*\*\*; Figure 8A,B). These results provide strong evidence supporting the underlying mechanism for the Snapin up-regulation effect on  $Ca_v1.3_L$  activity comes from an increase in the opening probability ( $P_o$ ) of  $Ca_v1.3_L$  channels.

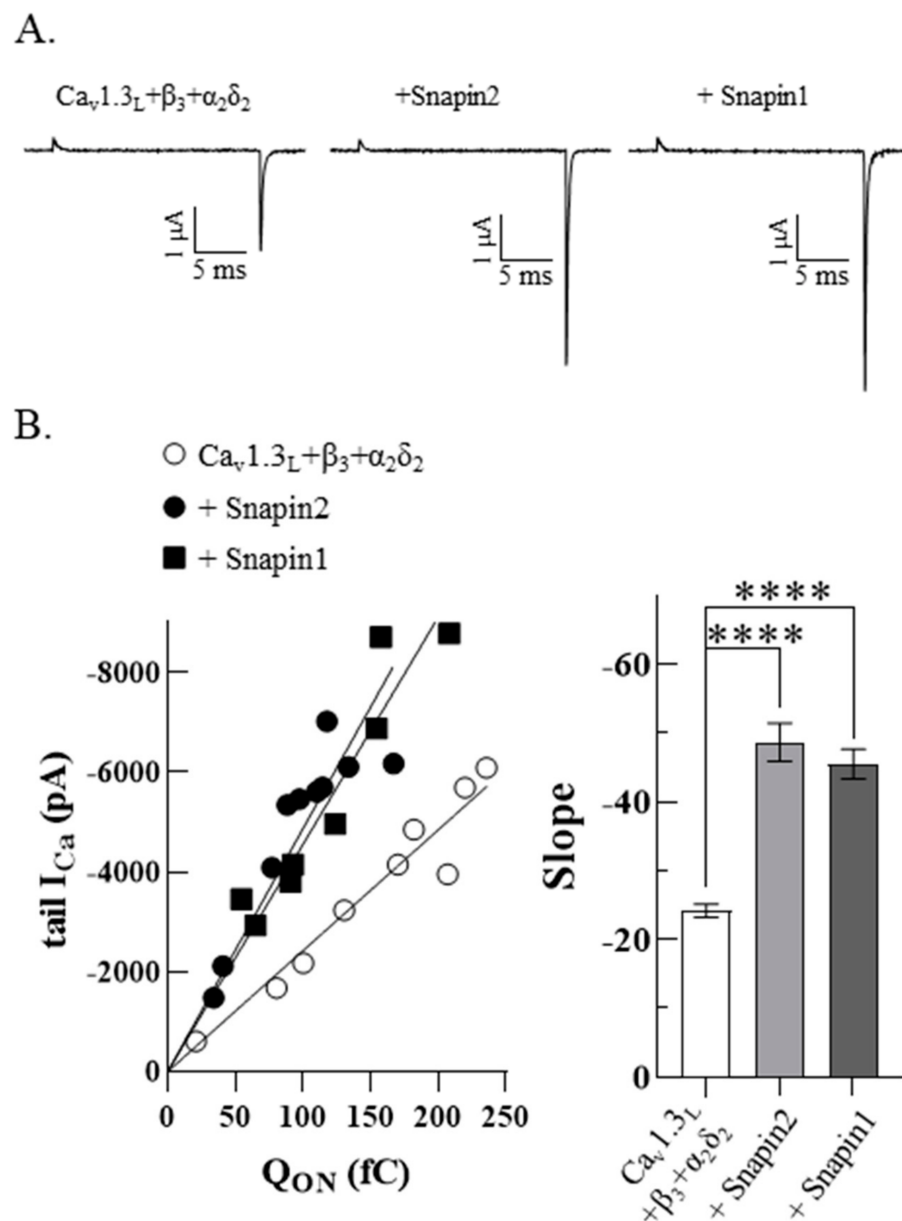


**Figure 8.** Increment of opening probability of  $Ca_v1.3_L$  channels by Snapin. (A) Representative gating current and tail current of  $Ca_v1.3_L/\beta_3/\alpha_2\delta_2$  co-expressed without or with Snapin 1 or 2. ON-gating currents were measured upon depolarizing to the virtual reversal potential from a holding potential of  $-80$  mV and tail currents were measured upon repolarizing to  $-80$  mV holding potential from the

same cells. **(B)** Correlation of ON-gating currents and tail currents.  $Q_{ON}$  (fC) values were plotted against tail current amplitudes (left panel,  $n = 8-10$ ). The slope values obtained from linear regression of data are  $-24.2 \pm 1.0$  for  $Ca_v1.3_L/\beta_3/\alpha_2\delta_2$ ,  $-48.7 \pm 2.7$  for  $Ca_v1.3_L/\beta_3/\alpha_2\delta_2$  plus Snapin2, and  $-45.5 \pm 2.2$  for  $Ca_v1.3_L/\beta_3/\alpha_2\delta_2$  plus Snapin1 and are represented as bar graphs. Statistical significances were tested with one-way ANOVA with Tukey's multiple comparison ( $p < 0.0001$ , \*\*\*\*).

### 3. Discussion

We here isolated rat Snapin2 as a molecular partner interacting with the  $CT_L$  of rat  $Ca_v1.3_L$  by utilizing Y2H screening. In the two different expression systems, both Snapin1 and Snapin2 enhanced  $Ca_v1.3_L$  channel activity, without altering other biophysical properties including voltage-dependent gating properties, current kinetics, and CDI. The unique interaction site of Snapin in  $CT_L$  was localized to a 24-amino-acid sequence, which belongs to exon 44, rendering the  $Ca_v1.3_L$  channels to be specifically up-regulated by Snapin. Furthermore, combined studies of luminometry and measurement of ON-gating and tail currents revealed that Snapin enhances the opening probability of the  $Ca_v1.3_L$  channel without changing the level of surface expression.

Our result showing that Snapin2 interacts with the  $CT_L$  of rat  $Ca_v1.3_L$  is consistent with a previous report in which rat Snapin1, a longer variant than Snapin2, interacted with the  $CT_L$  of human  $Ca_v1.3_L$  variant [30]. However, conflicting results were found in functional analysis of Snapin variants in expression systems. In our study, Snapin2 clearly up-regulated  $Ca_v1.3_L$  channel activity, whereas in the previous study, Snapin1 strongly down-regulated  $Ca_v1.3$  channel activity. In contrast with the down-regulation result in the previous study, our subsequent study showed that the Snapin1 variant also up-regulated  $Ca_v1.3_L$  channel activity.

To address possible causes for the conflicting results, we compared and analyzed patch-clamping data from the previous study with typical  $Ca_v1.3$  channel data in previous literature and from our experiments. First, we note the expression level and biophysical properties of  $Ca_v1.3$  channels. In the previous study, the currents estimated from HEK-293 cells stably expressing  $Ca_v1.3_L/\beta_{2a}/\alpha_2\delta$  were shown to be very small in average maximal current density ( $\sim 3$  pA/pF) and to be slowly activated upon +10 mV (or 0 mV) test potential [30]. The properties of  $Ca_v1.3$  current with tiny amplitude and slowly activating kinetics have not been shown in the other previous studies [11,33] or/and in our experiments. To use model cell lines to investigate voltage-activated ion channels, it is common knowledge that adequate expression levels and typical electrophysiological properties of certain channels would be primary prerequisites. To consider weak points, we also speculate that heterogeneity or impairment in the  $Ca_v1.3$  channel expression might lead to the low expression and abnormal property of the  $Ca_v1.3$  channel in the cell line used in the previous study. In addition, even if there is no causal relationship, only by considering the changes in the  $Ca_v1.3$  channel properties themselves, this implies that the experimental conditions were not appropriate. Second, we considered the suitability of HL-1 cells for studying  $Ca_v1.3$  channels. HL-1 cells, an atrial myocyte cell line, have been used for functional studies of T-type and L-type channels as well as atrial myocyte properties [34]. Among the L-type channels, the protein expression of the  $Ca_v1.2$  subunit was found to be greater than that of the  $Ca_v1.3$  subunit in the plasma membrane of HL-1 cells [34]. Thus, it can be inferred that the very small current ( $\sim 1$  pA/pF) was likely to be mainly permeated through the  $Ca_v1.2$  rather than the  $Ca_v1.3$  channel. This suggests that the HL-1 cell line is not suitable for  $Ca_v1.3$  regulation studies and raises the possibility that in the previous study, Snapin reduced  $Ca_v1.2$  channel activity via its interaction with the  $Ca_v1.2$  subunit. Thus, we tested the possibility of whether co-expression of Snapin1 with  $Ca_v1.2/\beta_3$  can increase  $Ca_v1.2$  channel activity in *Xenopus* oocytes. The experimental results from the oocytes showed that Snapin co-expression did not cause any statistically significant changes in the current amplitude and voltage-dependent gating properties of  $Ca_v1.2$  channels (Supplementary Figure S2). No regulation of  $Ca_v1.2$  current by Snapin1 does not support the tentative hypothesis and is contradictory to the previous

report addressing that Snapin1 down-regulated L-type channel activity by ~50% in HL-1 cells [30]. Even assuming that Snapin1 completely down-regulated  $Ca_v1.3$  activity, total L-type channel current in HL-1 cells should have been mildly down-regulated by Snapin1 because  $Ca_v1.2$  current in HL-1 cells would remain unaffected by Snapin1 (Supplementary Figure S2). Thus, we speculate that the contradictory effects might arise from Snapin-mediated nonspecific pathways, influencing channel activity of both L-type  $Ca_v1.2$  and  $Ca_v1.3$  isoforms.

We conducted further investigations to uncover the underlying mechanism for the Snapin up-regulation effect on  $Ca_v1.3_L$  using luminometry and immuno-cytochemistry to quantitate the surface and total expression of  $Ca_v1.3_L$  and electrophysiological measurements of ON-gating currents and tail currents at the reversal potential to estimate channel-opening probability ( $P_o$ ) [32]. Greater tail currents in the co-expression of Snapin were observed from comparable ON-gating currents. Analyzed from the relationships of ON-gating currents versus tail currents from the same cells, co-expression of Snapin induced about a 2-fold increase in the opening probability of  $Ca_v1.3_L$  channels, implying that the Snapin interaction exerted an effect that coupled charge movement to channel opening in a more efficient way. Combined with the results of no changes in the membrane and total expression, these results strongly suggest that Snapin can up-regulate  $Ca_v1.3_L$  channel activity through its specific association with long C-terminal  $Ca_v1.3_L$  variants, coupled with an increase of opening probability.

The Snapin interaction with SNAP25, one of the protein components composing SNARE complex, has been functionally relevant to facilitating transmitter release by increasing the number of priming and fusion synaptic vesicles [21,22,26,35] and inducing a fast exocytosis of large dense-core vesicles in chromaffin cells and insulin secretion of pancreatic beta cells [20,36,37]. Besides those roles of Snapin, we here report a novel role of Snapin, that is, an augmentation of  $Ca^{2+}$  entry through  $Ca_v1.3_L$  channels. Although it could be speculated simply that this role of Snapin may impact synaptic transmission and hormone secretion, it should be considered that the main  $Ca^{2+}$  channel types for synaptic release are N- and P/Q-type channels but not L-type channels [1]. Thus, we carefully suggest that this novel role of Snapin may cause a slight increase in the basal calcium levels of neurons. This can form favorable conditions for neuronal  $Ca^{2+}$  signaling pathways, which could plausibly lead to facilitation of basal synaptic transmission, modulation of gene expression, and neuronal development [1,8,38,39]. Nevertheless, in certain neuronal cells, such as cochlear inner hair cells and retinal bipolar cells, where  $Ca_v1.3$  channels are expressed [2,40], it is possible that the newly discovered role of Snapin directly contributes to facilitating synaptic transmission. Additionally, in adrenal chromaffin cells, where  $Ca_v1.3_L$  channels are expressed and involved in generation of pacemaking activity and catecholamine secretion [12], that the new role of Snapin may contribute to accelerating pacemaking activity and facilitating catecholamine secretion.

We conclude that Snapin2 specifically associates with long C-terminal  $Ca_v1.3$  variants and up-regulates the channel activity. The up-regulation effect of Snapin on  $Ca_v1.3_L$  arises from the increased opening probability without changes in the membrane and total expression. The enhanced  $Ca_v1.3$  activity in the presence of Snapin may be a novel mechanism underlying the facilitation effects of Snapin on synaptic transmission and hormone secretion.

## 4. Materials and Methods

### 4.1. Chemicals

Most of the chemicals were purchased from Sigma-Aldrich (St. Louis, MO, USA) and Thermo Fisher Scientific (Waltham, MA, USA). Minimal nutrients used for yeast-two-hybrid (Y2H) screenings were from Clontech (Mountain View, CA, USA).

#### 4.2. Yeast Two-Hybrid (Y2H) Screening

The long carboxyl terminus (CT<sub>L</sub>) of rat Ca<sub>v</sub>1.3<sub>L</sub> variant (GenBank accession no. NM\_001389225; Addgene plasmid no. 49332; Xu and Lipscomb, 2001) was amplified by PCR (polymerase chain reaction) and then cloned into bait pGBKT7 vector using NdeI and BamHI sites. CT<sub>L</sub>-pGBKT7 construct and rat brain cDNA library in pACT2 vector (Clontech) were co-transformed to AH109 competent cells to isolate novel proteins interacting with CT<sub>L</sub> using Matchmaker GAL4 yeast two-hybrid system (Clontech). A positive colony was selected on a high-stringent SD medium deficient of Leu, Trp, His, and Ade, in the presence of X-α-Gal. The vector insert in the positive clone was identified as including the full-length cDNA of rat Snapin2 (GenBank accession no. NM\_001025648). The Snapin2 cDNA was subcloned into pcDNA3 and pGEM-HEA vectors for co-expression studies in HEK293-cells and *Xenopus* oocytes, respectively.

The N-terminus (NT), I-II loop, II-III loop, and III-IV loop of Ca<sub>v</sub>1.3<sub>L</sub> and the short CT (CT<sub>S</sub>) of rat Ca<sub>v</sub>1.3<sub>S</sub> variant (Addgene plasmid number 49,333; GenBank accession no. AF370009; [10]) were also amplified by PCR and individually inserted into pGBKT7 bait vector. Their interaction with rat Snapin2 was tested by Y2H assays.

#### 4.3. Cloning of Rat Brain Snapin1

Rat brain cDNA was reverse-transcribed from rat brain total RNA (Clontech) using One-step RT-PCR kit (Qiagen, Hilden, Germany) according to the manufacturer's protocol. PCR was employed to amplify rat Snapin1 cDNA using forward and reverse primers (5'-GCGTCAGGGCAGTTCGC-3' and 5'-TTCTGTCTACCAAGACAAAGCTGT-3'). The PCR products were cloned into pCR2.1-TOPO vector (Invitrogen). One of the PCR products in pCR2.1-TOPO vector was analyzed by sequencing and then subcloned into pCDNA 3.1 vector using EcoRI and XbaI sites.

#### 4.4. Co-Expression of Snapin2 or Snapin1 with Ca<sub>v</sub>1.3 Variants in HEK-293 Cells

HEK-293 cells were cultured at 37 °C, 5% CO<sub>2</sub> in DMEM media containing 10% FBS, 1% penicillin, and streptomycin. Rat Snapin2- or Snapin1-pcDNA3 (or pcDNA3 null vector, control) was co-transfected into HEK-293 cells with cDNA mixture of rat Ca<sub>v</sub>1.3<sub>L</sub> (or Ca<sub>v</sub>1.3<sub>S</sub>), rat Ca<sub>v</sub>β<sub>3</sub> (GenBank accession no. M88751), and human Ca<sub>v</sub>α<sub>2</sub>δ<sub>2</sub> (GenBank accession no. NM\_006030) at equal molar ratio, together with 1/100 of eGFP-pcDNA3 construct using Effectene reagent (Qiagen) according to the provided protocol. Thirty-six hours after transfection, cells were dissociated from culture dishes with 0.25% trypsin-EDTA and plated on poly-L-lysine treated coverslips. Patch clamp recordings were performed between 48~72 h after transfection.

#### 4.5. Co-Expression of Snapin2 with Ca<sub>v</sub>1.3<sub>L</sub> in *Xenopus* Oocytes

Rat Ca<sub>v</sub>1.3<sub>L</sub>-pCDNA3 construct was linearized by *Avr*II at the 3' end. Rat β<sub>3</sub> and Snapin2 constructs were linearized by *Sac*II and *Afl*III, respectively. The linearized cDNAs were used as substrates for capped transcript synthesis using mMESSAGE mMACHINE T7 transcription kit (Ambion, Austin, TX USA) according to the manufacturer's instruction.

*Xenopus laevis* frogs were purchased from Hallym University (Chuncheon, Korea). As described previously [41], several ovary lobes were surgically isolated from female frogs, which were anesthetized. Follicles were subsequently eliminated from oocytes by digestion with collagenase (Gibco, 12 mg/mL) in a Ca<sup>2+</sup>-free OR2 solution (in mM: 82.5 NaCl, 2.5 KCl, 1 MgCl<sub>2</sub>, 5 HEPES; pH 7.6 with NaOH). Prior to cRNA injection, oocytes were recovered for several hours in a standard oocyte solution (in mM: 100 NaCl, 2 KCl, 1.8 CaCl<sub>2</sub>, 1 MgCl<sub>2</sub>, 5 HEPES, 2.5 pyruvic acid, and 50 mg/mL gentamicin; pH 7.6 with NaOH).

Snapin2 cRNA (or water) was co-injected with cRNA mixture of Ca<sub>v</sub>1.3<sub>L</sub> and Ca<sub>v</sub>β<sub>3</sub> at equal molar ratio using a Drummond Nanoject injector (Parkway, PA, USA). Current traces from *Xenopus* oocytes were recorded from the 4th day after injection.

#### 4.6. Electrophysiological Recordings in HEK-293 Cells

Whole-cell currents were measured with an Axopatch 200B patch clamp amplifier (Molecular Devices, Foster City, CA, USA) connected to a computer via a Digidata 1322A converter (Molecular Devices). The recording system and voltage-protocols were controlled using pCLAMP 9.2 software. Patch pipettes were pulled from borosilicate capillary tubing (World Precision Instruments, Sarasota, FL, USA) using PC-10 pipette puller (Narishige, Tokyo, Japan). When pipettes were filled with internal solution (in mM: 130 CsCl, 2 CaCl<sub>2</sub>, 10 HEPES, 10 EGTA, 5 MgATP; pH 7.3 with CsOH), the input resistance was 1.8–2.5 MΩ. The 10 mM CaCl<sub>2</sub> external solution was used for recordings (in mM: 140 TEACl, 2.5 CsCl, 10 CaCl<sub>2</sub>, 1 MgCl<sub>2</sub>, 10 HEPES; pH 7.3 with TEOH).

Current-voltage (*I-V*) relationship was obtained by 400-ms depolarizing step pulses from −60 mV to +70 mV by increments of 10 mV from a holding potential of −80 mV. Ca<sub>v</sub>1.3 currents were filtered at 2 kHz and sampled at 10 kHz. Ca<sup>2+</sup>-dependent inactivation (CDI) was quantified as the fraction (*r*<sub>50</sub>) of peak amplitude remaining after 50 ms plotted against various test potentials. Chord conductance values were calculated by the equation  $G = I/(V - V_{rev})$ , where *I* is the current amplitude at a test potential *V*, and *V*<sub>rev</sub> is the reversal potential. Channel availability was obtained by 10-s pre-pulses from −90 mV to −10 mV, followed by 0 mV test pulse from a holding potential of −80 mV.

Activation data were fitted by the Boltzmann equation:  $G = 1/[1 + \exp\{(V_{50,act} - V)/S_{act}\}]$ , where *V*<sub>50,act</sub> is the half-maximal activation potential, and *S*<sub>act</sub> is the slope conductance. Channel availability curves were fitted by the Boltzmann equation:  $I/I_{max} = 1/[1 + \exp\{(V_{50,inact} - V)/k\}]$ , where *I*<sub>max</sub> is maximal current amplitude, *V*<sub>50,inact</sub> is the half-inactivation potential, and *k* is the slope factor.

To estimate channel opening probability [32], ON-gating currents were measured by application of a 20-ms step pulse to the virtual reversal potential (+70~75 mV) and, from the same cells ionic tail currents (*I*<sub>tail</sub>), were measured upon repolarization to a holding potential of −80 mV. The capacitive linear properties were subtracted using −P/6 protocol. Data sampling for ON-gating currents was filtered at 10 KHz and sampled at 50 KHz. ON-gating currents at the reversal potential were represented as maximal charge movement values (*Q*<sub>ON</sub>), which were obtained from integrating the areas under ON-gating currents. The plots data of *Q*<sub>ON</sub> values versus tail current amplitudes corresponding to maximal conductance were regressed to yield slopes, which are approximate estimates of opening probability (*P*<sub>o</sub>).

#### 4.7. Electrophysiological Recordings in *Xenopus* Oocytes

A two-electrode voltage clamp method was applied to record Ca<sub>v</sub>1.3<sub>L</sub> current traces from *Xenopus* oocytes in 10 mM Ba<sup>2+</sup> recording solution (in mM: 90 NaOH, 1 KOH, 10 Ba(OH)<sub>2</sub>, 5 HEPES; pH 7.4 with CH<sub>3</sub>SO<sub>3</sub>H). Electrodes pulled from borosilicate capillary glass tubing (Warner Instrument, Holliston, MA) were filled with 3M KCl, and their resistance was 0.8~1.2 KΩ. Prior to current recordings, oocytes were injected with 40 mM BAPTA solution in a volume of 50 nL to eliminate endogenous Ca<sup>2+</sup> activated Cl<sup>−</sup> current. Ca<sub>v</sub>1.3 Ba<sup>2+</sup> currents were filtered at 1 kHz and sampled at 5 kHz. Data were analyzed with Clampfit 10.7 software and Prism software (GraphPad, San Diego, CA, USA).

#### 4.8. Construction and Luminometric Measurement of Ca<sub>v</sub>1.3<sub>L</sub>-HA

The hemagglutinin (HA) epitope was inserted between amino acids Q693 and T694 at the extracellular S5-pore loop of domain II by overlap extension PCR [42]. Snapin2-pCDNA3 (or empty pCDNA3) was co-transfected with Ca<sub>v</sub>1.3<sub>L</sub>-HA/β<sub>3</sub>/α<sub>2</sub>δ<sub>2</sub> constructs into HEK-293 cells using Effectene (Qiagen). Forty-eight hours after transfection, cells were washed with PBS and fixed in 4% paraformaldehyde for 5 min. A set of cell samples was permeabilized with 0.1% Triton X-100 for 5 min, and the other set was non-permeabilized without Triton treatment. After being washed three times with PBS, cells were incubated for 30 min in 2% bovine serum albumin solution for blocking and incubated in polyclonal rabbit anti-HA antibody for 1 h (1:200 dilution; 71–5500, Thermo Fisher Scientific). After

washings, cells were incubated with secondary goat anti-rabbit antibody conjugated with HRP (1:500 dilution; 170–6515, Bio-Rad) for 30 min and rinsed with PBS. After addition of SuperSignal ELISA femto maximum sensitivity substrates (Pierce, Rockford, IL, USA), the luminescence intensities of cells expressing  $\text{Ca}_v1.3_L\text{-HA}/\beta_3/\alpha_2\delta_2$  proteins were measured using EnSpire Multimode plate reader (PerkinElmer, Wellesley, MA, USA). The measured luminescence intensities were normalized with the amounts of protein in the individual wells determined by BCA assay.

#### 4.9. Immunocytochemistry Analysis

Snapin2-pCDNA3 (or empty pCDNA3) was co-transfected with  $\text{Ca}_v1.3_L\text{-HA}/\beta_3/\alpha_2\delta_2$  constructs into HEK-293 cells. After 48 h, cells were washed with PBS and fixed with 4% paraformaldehyde for 5 min. After washing, two sets of cells were blocked with 2% bovine serum albumin (BSA) for 30 min, followed by overnight incubation polyclonal rabbit anti-HA antibody (1:200 dilution; 71–5500, Thermo Fisher Scientific) with 0.1% BSA at 4 °C. On the next day, cells were washed with PBS and incubated with FITC-conjugated goat anti-rabbit IgG antibodies (1:500 dilution; sc-2012, Santa Cruz, CA, USA) for 1 h. Cells were washed with PBS and covered with slides. Fluorescence images were taken using a confocal microscope (ZEISS LMS 880, Oberkochen, Germany). Line-scan analysis of the cell fluorescence images was obtained using ZEISS ZEN software and exhibited as relative fluorescence intensity (arbitrary unit, a.u.).

#### 4.10. Statistical Analysis

All data values are presented as mean  $\pm$  S.E.M. Statistical significances were evaluated using Student's unpaired *t*-test or one-way ANOVA combined with Tukey's multiple comparison tests, with  $p < 0.05$  (\*),  $p < 0.01$  (\*\*),  $p < 0.001$  (\*\*\*), and  $p < 0.0001$  (\*\*\*\*) as levels of significance.

**Supplementary Materials:** The followings are available online at <https://www.mdpi.com/article/10.3390/ijms222011268/s1>, Figure S1: No regulatory effect of Snapin1 on  $\text{Ca}_v1.3_S$ . Figure S2: Snapin1 did not alter  $\text{Ca}_v1.2$  channel activity in *Xenopus* oocytes.

**Author Contributions:** Conceptualization, S.J. and J.-H.L.; methodology, S.J. and J.-H.L.; formal analysis, S.J. and J.-H.L.; investigation, S.J. and J.-H.L.; resources, S.J. and J.-H.L.; data curation, S.J.; writing—original draft preparation, S.J., J.-S.R. and J.-H.L.; writing—review and editing, S.J., J.-S.R. and J.-H.L.; visualization, S.J. and J.-H.L.; supervision, J.-H.L.; project administration, J.-H.L.; funding acquisition, J.-H.L. All authors have read and agreed to the published version of the manuscript.

**Funding:** This work was supported by the Basic Science Research Program [2018R1D1A1B07043142] and the Priority Research Centers Program [2009-0093822] through the National Research Foundation of Korea (NRF), and a Special grant from Sogang University [202119028] to J.-H. Lee.

**Institutional Review Board Statement:** *Xenopus* oocytes were maintained and prepared according to a standard protocol approved by Sogang University Animal Committee (SGU2013-03).

**Informed Consent Statement:** Not applicable.

**Data Availability Statement:** The data that support for this publication are available from the corresponding author under reasonable request.

**Acknowledgments:** The authors thank Ho-Won Kang for his initial Y2H screening.

**Conflicts of Interest:** The authors declare that there is no conflict of interest for this research.

## References

1. Dolphin, A.C.; Lee, A. Presynaptic calcium channels: Specialized control of synaptic neurotransmitter release. *Nat. Rev. Neurosci.* **2020**, *21*, 213–229. [[CrossRef](#)] [[PubMed](#)]
2. Platzer, J.; Engel, J.; Schrott-Fischer, A.; Stephan, K.; Bova, S.; Chen, H.; Zheng, H.; Striessnig, J. Congenital deafness and sinoatrial node dysfunction in mice lacking class D L-type  $\text{Ca}^{2+}$  channels. *Cell* **2000**, *102*, 89–97. [[CrossRef](#)]
3. Mangoni, M.E.; Couette, B.; Bourinet, E.; Platzer, J.; Reimer, D.; Striessnig, J.; Nargeot, J. Functional role of L-type  $\text{Ca}_v1.3$   $\text{Ca}^{2+}$  channels in cardiac pacemaker activity. *Proc. Natl. Acad. Sci. USA* **2003**, *100*, 5543–5548. [[CrossRef](#)] [[PubMed](#)]

4. Bech-Hansen, N.T.; Naylor, M.J.; Maybaum, T.A.; Pearce, W.G.; Koop, B.; Fishman, G.A.; Mets, M.; Musarella, M.A.; Boycott, K.M. Loss-of-function mutations in a calcium-channel alpha1-subunit gene in Xp11.23 cause incomplete X-linked congenital stationary night blindness. *Nat. Genet.* **1998**, *19*, 264–267. [[CrossRef](#)] [[PubMed](#)]
5. Namkung, Y.; Skrypnik, N.; Jeong, M.J.; Lee, T.; Lee, M.S.; Kim, H.L.; Chin, H.; Suh, P.G.; Kim, S.S.; Shin, H.S. Requirement for the L-type Ca<sup>2+</sup> channel alpha(1D) subunit in postnatal pancreatic beta cell generation. *J. Clin. Investig.* **2001**, *108*, 1015–1022. [[CrossRef](#)]
6. Kim, S.H.; Park, Y.R.; Lee, B.; Choi, B.; Kim, H.; Kim, C.H. Reduction of Ca<sub>v</sub>1.3 channels in dorsal hippocampus impairs the development of dentate gyrus newborn neurons and hippocampal-dependent memory tasks. *PLoS ONE* **2017**, *12*, e0181138.
7. Azizan, E.A.B.; Poulsen, H.; Tuluc, P.; Zhou, J.; Clausen, M.V.; Lieb, A.; Maniero, C.; Garg, S.; Bochukova, E.G.; Zhao, W.; et al. Somatic mutations in ATP1A1 and CACNA1D underlie a common subtype of adrenal hypertension. *Nat. Genet.* **2013**, *45*, 1055–1060. [[CrossRef](#)]
8. Pinggera, A.; Striessnig, J. Ca<sub>v</sub>1.3 (CACNA1D) L-type Ca<sup>2+</sup> channel dysfunction in CNS disorders. *J. Physiol.* **2016**, *594*, 5839–5849. [[CrossRef](#)]
9. Pinggera, A.; Mackenroth, L.; Rump, A.; Schallner, J.; Beleggia, F.; Wollnik, B.; Striessnig, J. New gain-of-function mutation shows CACNA1D as recurrently mutated gene in autism spectrum disorders and epilepsy. *Hum. Mol. Genet.* **2017**, *26*, 2923–2932. [[CrossRef](#)]
10. Xu, W.; Lipscombe, D. Neuronal Ca<sub>v</sub>1.3alpha1 L-type channels activate at relatively hyperpolarized membrane potentials and are incompletely inhibited by dihydropyridines. *J. Neurosci. Off. J. Soc. Neurosci.* **2001**, *21*, 5944–5951. [[CrossRef](#)]
11. Singh, A.; Gebhart, M.; Fritsch, R.; Sinnegger-Brauns, M.J.; Poggiani, C.; Hoda, J.C.; Engel, J.; Romanin, C.; Striessnig, J.; Koschak, A. Modulation of voltage- and Ca<sup>2+</sup>-dependent gating of Ca<sub>v</sub>1.3 L-type calcium channels by alternative splicing of a C-terminal regulatory domain. *J. Biol. Chem.* **2008**, *283*, 20733–20744. [[CrossRef](#)]
12. Vandael, D.H.; Marcantoni, A.; Carbone, E. Ca<sub>v</sub>1.3 Channels as Key Regulators of Neuron-Like Firings and Catecholamine Release in Chromaffin Cells. *Curr. Mol. Pharmacol.* **2015**, *8*, 149–161. [[CrossRef](#)]
13. Toyoda, F.; Mesirca, P.; Dubel, S.; Ding, W.G.; Striessnig, J.; Mangoni, M.E.; Matsuura, H. Ca<sub>v</sub>1.3 L-type Ca<sup>2+</sup> channel contributes to the heartbeat by generating a dihydropyridine-sensitive persistent Na<sup>+</sup> current. *Sci. Rep.* **2017**, *7*, 7869. [[CrossRef](#)]
14. McKinney, B.C.; Sze, W.; Lee, B.; Murphy, G.G. Impaired long-term potentiation and enhanced neuronal excitability in the amygdala of Ca<sub>v</sub>1.3 knockout mice. *Neurobiol. Learn. Mem.* **2009**, *92*, 519–528. [[CrossRef](#)]
15. Vivas, O.; Moreno, C.M.; Santana, L.F.; Hille, B. Proximal clustering between BK and Ca<sub>v</sub>1.3 channels promotes functional coupling and BK channel activation at low voltage. *eLife* **2017**, *6*, e28029. [[CrossRef](#)]
16. Stanika, R.I.; Flucher, B.E.; Obermair, G.J. Regulation of Postsynaptic Stability by the L-type Calcium Channel Ca<sub>v</sub>1.3 and its Interaction with PDZ Proteins. *Curr. Mol. Pharmacol.* **2015**, *8*, 95–101. [[CrossRef](#)] [[PubMed](#)]
17. Ilardi, J.M.; Mochida, S.; Sheng, Z.H. Snapin: A SNARE-associated protein implicated in synaptic transmission. *Nat. Neurosci.* **1999**, *2*, 119–124. [[CrossRef](#)] [[PubMed](#)]
18. Chheda, M.G.; Ashery, U.; Thakur, P.; Rettig, J.; Sheng, Z.H. Phosphorylation of Snapin by PKA modulates its interaction with the SNARE complex. *Nat. Cell Biol.* **2001**, *3*, 331–338. [[CrossRef](#)]
19. Vites, O.; Rhee, J.S.; Schwarz, M.; Rosenmund, C.; Jahn, R. Reinvestigation of the role of snapin in neurotransmitter release. *J. Biol. Chem.* **2004**, *279*, 26251–26256. [[CrossRef](#)]
20. Tian, J.H.; Wu, Z.X.; Unzicker, M.; Lu, L.; Cai, Q.; Li, C.; Schirra, C.; Matti, U.; Stevens, D.; Deng, C.; et al. The role of Snapin in neurosecretion: Snapin knock-out mice exhibit impaired calcium-dependent exocytosis of large dense-core vesicles in chromaffin cells. *J. Neurosci. Off. J. Soc. Neurosci.* **2005**, *25*, 10546–10555. [[CrossRef](#)] [[PubMed](#)]
21. Pan, P.Y.; Tian, J.H.; Sheng, Z.H. Snapin facilitates the synchronization of synaptic vesicle fusion. *Neuron* **2009**, *61*, 412–424. [[CrossRef](#)] [[PubMed](#)]
22. Dickman, D.K.; Tong, A.; Davis, G.W. Snapin is critical for presynaptic homeostatic plasticity. *J. Neurosci. Off. J. Soc. Neurosci.* **2012**, *32*, 8716–8724. [[CrossRef](#)] [[PubMed](#)]
23. Buxton, P.; Zhang, X.M.; Walsh, B.; Sriratana, A.; Schenberg, I.; Manickam, E.; Rowe, T. Identification and characterization of Snapin as a ubiquitously expressed SNARE-binding protein that interacts with SNAP23 in non-neuronal cells. *Biochem. J.* **2003**, *375*, 433–440. [[CrossRef](#)] [[PubMed](#)]
24. Cai, Q.; Lu, L.; Tian, J.H.; Zhu, Y.B.; Qiao, H.; Sheng, Z.H. Snapin-regulated late endosomal transport is critical for efficient autophagy-lysosomal function in neurons. *Neuron* **2010**, *68*, 73–86. [[CrossRef](#)]
25. Lee, H.H.; Nemecek, D.; Schindler, C.; Smith, W.J.; Ghirlando, R.; Steven, A.C.; Bonifacino, J.S.; Hurley, J.H. Assembly and architecture of biogenesis of lysosome-related organelles complex-1 (BLOC-1). *J. Biol. Chem.* **2012**, *287*, 5882–5890. [[CrossRef](#)]
26. Di Giovanni, J.; Sheng, Z.H. Regulation of synaptic activity by snapin-mediated endolysosomal transport and sorting. *EMBO J.* **2015**, *34*, 2059–2077. [[CrossRef](#)]
27. Zissimopoulos, S.; West, D.J.; Williams, A.J.; Lai, F.A. Ryanodine receptor interaction with the SNARE-associated protein snapin. *J. Cell Sci.* **2006**, *119*, 2386–2397. [[CrossRef](#)]
28. Mistry, A.C.; Mallick, R.; Klein, J.D.; Weimbs, T.; Sands, J.M.; Fröhlich, O. Syntaxin specificity of aquaporins in the inner medullary collecting duct. *Am. J. Physiology. Ren. Physiol.* **2009**, *297*, 292–300. [[CrossRef](#)]
29. Goswami, C.; Rademacher, N.; Smalla, K.H.; Kalscheuer, V.; Ropers, H.H.; Gundelfinger, E.D.; Hucho, T. TRPV1 acts as a synaptic protein and regulates vesicle recycling. *J. Cell Sci.* **2010**, *123*, 2045–2057. [[CrossRef](#)]

30. Sun, X.L.; Yuan, J.F.; Jin, T.; Cheng, X.Q.; Wang, Q.; Guo, J.; Zhang, W.; Zhang, Y.; Lu, L.; Zhang, Z. Physical and functional interaction of Snapin with Ca<sub>v</sub>1.3 calcium channel impacts channel protein trafficking in atrial myocytes. *Cell. Signal.* **2017**, *30*, 118–129. [[CrossRef](#)]
31. Kang, H.W.; Park, J.Y.; Lee, J.H. Molecular cloning and characterization of a hamster Ca<sub>v</sub>1.3 Ca<sup>2+</sup> channel variant with a long carboxyl terminus. *Biochim. Biophys. Acta* **2011**, *1808*, 1629–1638. [[CrossRef](#)] [[PubMed](#)]
32. Bock, G.; Gebhart, M.; Scharinger, A.; Jangsangthong, W.; Busquet, P.; Poggiani, C.; Sartori, S.; Mangoni, M.E.; Sinnegger-Brauns, M.J.; Herzig, S.; et al. Functional properties of a newly identified C-terminal splice variant of Ca<sub>v</sub>1.3 L-type Ca<sup>2+</sup> channels. *J. Biol. Chem.* **2011**, *286*, 42736–42748. [[CrossRef](#)]
33. Zhang, H.; Fu, Y.; Altier, C.; Platzer, J.; Surmeier, D.J.; Bezprozvanny, I. Ca<sub>v</sub>1.2 and Ca<sub>v</sub>1.3 neuronal L-type calcium channels: Differential targeting and signaling to pCREB. *Eur. J. Neurosci.* **2006**, *23*, 2297–2310. [[CrossRef](#)] [[PubMed](#)]
34. Scharinger, A.; Eckrich, S.; Vandael, D.H.; Schönig, K.; Koschak, A.; Hecker, D.; Kaur, G.; Lee, A.; Sah, A.; Bartsch, D.; et al. Cell-type-specific tuning of Ca<sub>v</sub>1.3 Ca<sup>2+</sup>-channels by a C-terminal automodulatory domain. *Front. Cell. Neurosci.* **2015**, *9*, 309. [[CrossRef](#)]
35. Banerjee, R.; Yoder, J.B.; Yue, D.T.; Amzel, L.M.; Tomaselli, G.F.; Gabelli, S.B.; Ben-Johny, M. Bilobal architecture is a requirement for calmodulin signaling to Ca<sub>v</sub>1.3 channels. *Proc. Natl. Acad. Sci. USA* **2018**, *115*, 3026–3035. [[CrossRef](#)]
36. Xia, M.; Salata, J.J.; Figueroa, D.J.; Lawlor, A.M.; Liang, H.A.; Liu, Y.; Connolly, T.M. Functional expression of L- and T-type Ca<sup>2+</sup> channels in murine HL-1 cells. *J. Mol. Cell. Cardiol.* **2004**, *36*, 111–119. [[CrossRef](#)] [[PubMed](#)]
37. Yu, S.C.; Klosterman, S.M.; Martin, A.A.; Gracheva, E.O.; Richmond, J.E. Differential roles for snapin and synaptotagmin in the synaptic vesicle cycle. *PLoS ONE* **2013**, *8*, e57842. [[CrossRef](#)]
38. Song, W.J.; Seshadri, M.; Ashraf, U.; Mdluli, T.; Mondal, P.; Keil, M.; Azevedo, M.; Kirschner, L.S.; Stratakis, C.A.; Hussain, M.A. Snapin mediates incretin action and augments glucose-dependent insulin secretion. *Cell Metab.* **2011**, *13*, 308–319. [[CrossRef](#)]
39. Schmidt, T.; Schirra, C.; Matti, U.; Stevens, D.R.; Rettig, J. Snapin accelerates exocytosis at low intracellular calcium concentration in mouse chromaffin cells. *Cell Calcium* **2013**, *54*, 105–110. [[CrossRef](#)]
40. Ma, H.; Cohen, S.; Li, B.; Tsien, R.W. Exploring the dominant role of Cav1 channels in signalling to the nucleus. *Biosci. Rep.* **2012**, *33*, 97–101. [[CrossRef](#)]
41. Marschallinger, J.; Sah, A.; Schmuckermair, C.; Unger, M.; Rotheneichner, P.; Kharitonova, M.; Waclawiczek, A.; Gerner, P.; Jaksch-Bogensperger, H.; Berger, S.; et al. The L-type calcium channel Ca<sub>v</sub>1.3 is required for proper hippocampal neurogenesis and cognitive functions. *Cell Calcium* **2015**, *58*, 606–616. [[CrossRef](#)] [[PubMed](#)]
42. Shi, L.; Chang, J.Y.-A.; Yu, F.; Ko, M.L.; Ko, G.Y.P. The Contribution of L-Type Ca<sub>v</sub>1.3 Channels to Retinal Light Responses. *Front. Mol. Neurosci.* **2017**, *10*, 394. [[CrossRef](#)]